AIP | Review of Scientific Instruments

A generic "micro-Stoney" method for the measurement of internal stress and elastic modulus of ultrathin films

Audrey Favache, Sophie Ryelandt, Maxime Melchior, Gul Zeb, Pierre Carbonnelle, Jean-Pierre Raskin, and Thomas Pardoen

Citation: Review of Scientific Instruments **87**, 015002 (2016); doi: 10.1063/1.4939912
View online: http://dx.doi.org/10.1063/1.4939912
View Table of Contents: http://scitation.aip.org/content/aip/journal/rsi/87/1?ver=pdfcov
Published by the AIP Publishing

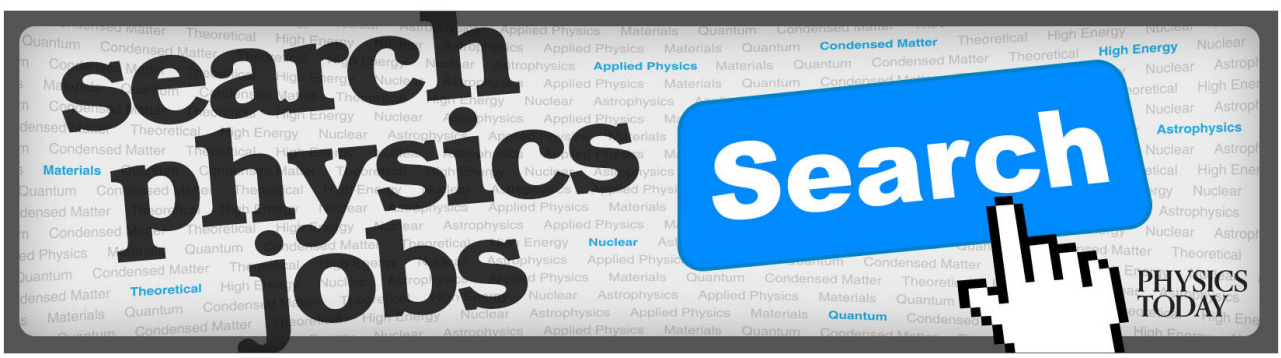

A generic "micro-Stoney" method for the measurement of internal stress and elastic modulus of ultrathin films

Audrey Favache,[1] Sophie Ryelandt,[1] Maxime Melchior,[1] Gul Zeb,[2] Pierre Carbonnelle,[3] Jean-Pierre Raskin,[3] and Thomas Pardoen[1]
[1]*Institute of Mechanics, Materials and Civil Engineering, Université catholique de Louvain, Place Sainte Barbe 2 L5.02.02, 1348 Louvain-la-Neuve, Belgium*
[2]*Centre de Collaboration MiQro Innovation (C2MI), Bromont, Québec J2L 1S8, Canada*
[3]*Information and Communications Technologies, Electronics and Applied Mathematics (ICTEAM), Microwave Laboratory, Université catholique de Louvain, 1348 Louvain-la-Neuve, Belgium*

(Received 5 October 2015; accepted 3 January 2016; published online 20 January 2016)

Accurate measurement of the mechanical properties of ultra-thin films with thicknesses typically below 100 nm is a challenging issue with an interest in many fields involving coating technologies, microelectronics, and MEMS. A bilayer curvature based method is developed for the simultaneous determination of the elastic mismatch strain and Young's modulus of ultra-thin films. The idea is to deposit the film or coating on very thin cantilevers in order to amplify the curvature compared to a traditional "Stoney" wafer curvature test, hence the terminology "micro-Stoney." The data reduction is based on the comparison of the curvatures obtained for different supporting layer thicknesses. The elastic mismatch strain and Young's modulus are obtained from curvature measurements of cantilevers before and after the film deposition. The data reduction scheme relies on both analytical and finite element calculations, depending on the magnitude of the curvature. The experimental validation has been performed on ultra-thin low pressure chemical vapor deposited silicon nitride films with thickness ranging between 54 and 133 nm deposited on silicon cantilevers. The technique is sensitive to the cantilever geometry, in particular, to the thickness ratio and width/thickness ratio. Therefore, the precision in the determination of the latter quantities determines the accuracy on the extracted elastic mismatch strain and elastic modulus. The method can be potentially applied to films as thin as a few nanometers. © *2016 AIP Publishing LLC.* [http://dx.doi.org/10.1063/1.4939912]

I. INTRODUCTION

The measurement of mechanical properties, involving the determination of the magnitude of the internal stress and elastic modulus, of extremely thin films especially below 100 nm is a challenging task for which no generic, versatile, and accurate approach has been developed up to now. However, these data are essential in the context of many advanced technologies relying on a proper control of the state of internal stress and of the stiffness of the films and coatings used for their functional and/or mechanical properties. This is true in a variety of microelectronic devices, micro-electromechanical systems, protective coatings, and/or magnetic recording systems.[1,2] One difficulty is that mechanical properties are size dependent at these length scales, as well as process dependent. Hence, experimental characterization is always required to ensure that the target performances are attained. Here, we propose and validate a method derived from the classical "Stoney"-type measurement to characterize both the internal stress and the elastic modulus of extremely thin films, i.e., a few hundreds down to a few tens of nanometers. More detailed reviews on thin film characterization techniques may be found, for instance, in Refs. 2–5; the review below is only a brief coverage of the existing techniques to evaluate these two quantities.

The generation of internal stress in thin films results from various phenomena and depends on the deposition conditions.[6–8] The internal stress is an important parameter with respect, for instance, to microstructure stability and to cracking or delamination resistance. When a film is released from its substrate to produce different types of bridges, cantilevers, or membranes, the relaxation of the internal stress leads to elastic deformations, possible buckling instabilities, and, in any cases of multilayered films, to curved configurations which may take complex shapes if the stresses are sufficiently high.

Numerous techniques can be found in the literature for measuring the internal stress in thin films, the most common being based either on measuring a change in the lattice constants of the material or on measuring the change in the stress induced curvature of bent structures. Among the first category, X-ray diffraction provides the state of biaxial internal stress.[9,10] Raman spectroscopy can be used to estimate the elastic strain from which the stress can be extracted if the elastic modulus is known.[11] Curvature measurement methods are the most widely applied methods for measuring internal stress in films lying on flat substrates, since they can be performed *in situ* and on non-crystalline materials. The change in curvature can be measured using interferometry or profilometry methods.[12,13] Stoney's equation relating the substrate curvature to the film stress has been used in its original or modified form for more than 100 yr[6,14,15] and allows the determination of the internal stress without prior knowledge of the film modulus. Substrates in the form of cantilevers combined to multi-beam optical

stress (MOS) sensors have been used for characterizing film stress.[15–17] Still, estimating the internal stress of films thinner than 50 nm remains a challenge, in addition to the fact that MOS sensors are not adapted to all experimental conditions. There is, therefore, a need for a method that may be applied to any deposition instruments and conditions. Aside from this first set of methods, micro-machined structures of various geometries have been developed to measure the internal strain of thin films by measuring the displacement of these structures upon release of the underlying layer.[18,19] Retrieving the corresponding stress requires the knowledge of the elastic modulus, which has to be independently determined.

Many design issues related to the overall stiffness, resonance frequency, stored elastic energy, wear resistance, or buckling load depend on the elastic properties of the films. Various methods for characterizing elastic modulus for freestanding and supported films have been developed, involving conventional tensile tests, contact, dynamic, acoustic, and curvature based methods. Following the conventional testing approach used for bulk materials, uniaxial micro-tensile tests have been developed to characterize the material response in small scale specimens (e.g., Refs. 19–29). The so-called bulge test[30,31] and four-point bending test[32] are other techniques borrowed from macroscopic testing methods.

A widely used contact method for measuring the elastic modulus at small scales is nanoindentation.[33] However, in thin film indentation, the indentation depth is often limited to typically less than 10% of the film thickness,[34–36] which makes very challenging the extraction of the elastic modulus in films thinner than typically 200 nm, especially if the surface is not perfectly flat because roughness effects perturb measurements at shallow indentation depths. A load-deflection test employing a surface profiler has also been developed to characterize the elastic modulus on various test structures, e.g., cantilevers, doubly supported bridges, and bridge-sliders.[37,38]

Dynamic methods are based on the measurement of the resonance frequency of structures. Photo-thermal, acoustic, piezoelectric, or mechanical methods have been developed to vibrate the test structures.[39–42] These methods allow the testing of multilayers or of connected beam structures. However, the uncertainty in the results for films thinner than 200 nm significantly increases.

Acoustic methods are based on the generation and propagation of wave pulses in the film. The most used techniques for thin films include Raman-Brillouin diffusion and ultrafast acoustics. Surface Brillouin scattering is gaining interest for the determination of the elastic constants of opaque thin films,[43] but it is difficult to use in the case of semi-transparent films on substrates. Recent developments in picosecond ultrasonics allow the measurement of sound velocities in submicronic layers and multilayers typically thicker than 100 nm from which the elastic properties can be retrieved.[44,45]

Previously, our group has reported the extraction of Young's modulus of thin films by combining a stress measurement in a fully unrelaxed condition using Stoney's equation and a strain measurement after complete relaxation after release.[13] Young's modulus was obtained from the ratio of totally unrelaxed stress to the corresponding deposition induced strain.

Few methods exist that allow extracting simultaneously the internal stress and the elastic modulus. For instance, Osterberg *et al.* proposed a technique using pull-in instabilities on MEMS structures for measuring the elastic modulus and the internal stress,[46] which has been applied to measure the Young's modulus of silicon cantilevers with thickness in the range of 40 nm–1 μm.[47] The previously mentioned bulge test can also be used to simultaneously measure the modulus and the internal stress of thin films.[48,49]

The present paper describes a combined modulus and stress measurement methodology which extends the work of Boé *et al.*[13] and with the objective to be accurate for very thin films. As explained in Section II, the thin film material is deposited on thin silicon cantilevers in order to enhance the sensitivity of the method. Lithography methods are used to fabricate the specimens. Curvature measurements are made either by interferometry or using scanning electronic microscopy (SEM) images. This non-contact type measurement method, together with the use of an analytical and finite element (FE) model of the thermo-elastic deformation of bilayers (described in Section III), allows generating accurate results even for tens of nanometer thick films, by applying the data reduction scheme presented in Section IV. The two main advantages of the method are (i) the capacity to extract the Young's modulus in very thin films while the above-mentioned techniques are mainly limited to thicknesses larger than 100-200 nm and (ii) there is no need to fabricate single layer freestanding cantilevers or membranes, which poses experimental difficulties when the thickness is below 100 nm. In the technique proposed here, since measurements are made on bilayer cantilevers, the film material is still supported by the substrate material and the structures are thicker than 100 nm, even if the film is much thinner. Hence, contrary to the existing techniques, the "micro-Stoney" approach allows the measurement of the Young's modulus of films of a few tens of nanometer thickness. Note also that the measurement of fully relaxed stress for few tens of nanometer thick films using the classical curvature method is not sensitive enough for very thin films possessing relatively low internal stresses. The use of a bilayer cantilever as it is presented here reduces the thickness of the substrate with respect to the film thickness, resulting in much larger curvature changes and hence an enhanced sensitivity. The approach is validated on experimental results obtained on thin silicon nitride (Si_3N_4) films in Section V.

II. EXPERIMENTAL SETUP

The test structures are fabricated on silicon-on-insulator (SOI) wafers following two UV lithography steps along the [110] direction of the top silicon (Si) layer. First, Si cantilevers are patterned into the top Si layer of the SOI wafer through reactive ion etching (RIE) using a SF_6 based plasma. Then, a Si_3N_4 is deposited at 790 °C by low pressure chemical vapor deposition (LPCVD) in a vertical Koyo VF-1000LP furnace and a second lithography is performed using RIE with a $SF_6/SiCl_4$ based plasma. The two etching steps are performed in an Electrotech Plasmafab 310/340 equipment. This allows fabricating cantilevers made either of a Si single

layer, of a Si_3N_4 single layer, or of a Si/Si_3N_4 bilayer. Silicon oxide (SiO_2) acts as the etch stop layer for the two etching steps. Since UV light for the photolithography process offers a resolution of 0.5 μm, cantilevers of 10 ± 0.5 μm width and various lengths ranging from 100 μm to 1900 μm have been fabricated to ensure the reproducibility and consistency of the measurements. Finally, the structures are wet released using HF (73%) to etch the SiO_2 sacrificial layer. A schematic representation of the fabrication steps and of the obtained structures is given in Figure 1, with the Si_3N_4 layer being the test material in this study.

Two sets of samples have been processed on SOI wafers:

1. The "P"-series: LPCVD Si_3N_4 films with a constant film thickness are deposited on silicon top layers of SOI wafers with different thicknesses equal to 140 nm, 400 nm, and 700 nm (before release). The etching time of the HF release was 3 min for all samples.
2. The "G"-series: a LPCVD Si_3N_4 with ~150 nm thickness has been deposited on the Si top layers of a SOI wafer with a Si thickness of 400 nm. As HF also etches Si_3N_4 at comparatively smaller rate than SiO_2,[50] it was exploited to deliberately alter the film thickness, after cutting the wafer into several samples before the release step and using different release times for each of the wafer dies. Si_3N_4 films of thicknesses ranging from 46 to 133 nm after release on 400 nm Si were produced.

The film and substrate thicknesses were measured before and after release by ellipsometry using a Cauchy model. SEM and interferometry have been used to determine the radii of curvature of the Si/Si_3N_4 cantilevers. SEM imaging using a Zeiss Ultra 55 FEG-SEM was appropriate to generate precise measurements on beams exhibiting very strong curling such as shown in Figure 2. White light interferometry measurements have been performed in a MSA-500 Micro System Analyzer from Polytec. Interferometry is well adapted to measure curvature radii such that the cantilevers are not curled more than the quarter of a circle, i.e., for radii more than $2/\pi$ times the length of the cantilever. For 100 to 1900 μm long cantilevers, this corresponds to minimal radii in the range of approximately 65 to 1200 μm. The radii of curvature are then extracted through a quadratic interpolation of the line profile of the cantilevers across the long axis.

III. FINITE ELEMENT SIMULATIONS

FE simulations of the mechanical behavior of the bilayers upon release have been carried out using the Oofelie::Multiphysics software based on the nonlinear solver. Rectangular bilayer beams with length $L = 200$ μm and width $W = 10$ μm have been meshed using hexahedrons with quadratic interpolation. From symmetry, only one half of the cantilever width has been modelled with perfect clamping at one of the extremities. A convergence study showed that a mesh involving 160 elements over the length, 15 elements over the half width, and 1 element over the thickness in each layer was sufficient to ensure convergence on the predicted curvature.

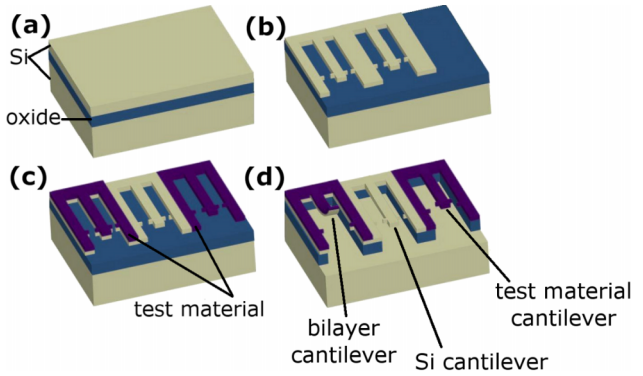

FIG. 1. Schematic representation of the main fabrication steps of the test structures. Starting (a) with a SOI wafer, (b) fabrication of Si cantilevers through a first lithography and etching procedure, (c) deposition and patterning of the test material through a second lithography and etching procedure, (d) etching sacrificial layer to release test structures.

The film of interest (Si_3N_4) has been considered to behave as an isotropic elastic material, whereas the supporting Si layer has been taken orthotropic, accounting for the elastic anisotropy of the Si crystal structure. The elastic constants of Si in the reference frame of a (100) wafer have been taken from Ref. 51 as equal to $[E_x, E_y, E_z] = [169, 169, 130]$ GPa for the elastic modulus, $[\nu_{xy}, \nu_{yz}, \nu_{zx}] = [0.064, 0.36, 0.28]$ for the Poisson ratio and $[G_{xy}, G_{yz}, G_{zx}] = [50.9, 79.6, 79.6]$ GPa for the shear modulus. In agreement with the experimental structures, the cantilever is oriented along the x-axis ([110] direction), i.e., parallel to the flat of the wafer.

The bending of the cantilever results from the difference existing, before release, between the elastic strain stored in the upper layer ε_f and the elastic strain in the bottom layer ε_s. The difference in elastic strain, noted $\Delta\varepsilon = \varepsilon_f - \varepsilon_s$, is the driving force for the bending of the bilayer upon release until force and moment equilibrium is reached. The elastic strains ε_s and ε_f come from a mismatch strain in each layer which may have various origins such as epitaxial strain, growth strain, and/or thermal expansion.[2] Without loss of generality, $\Delta\varepsilon$ is induced in the simulations by applying a fictitious uniform temperature change to the beam that was initially free of constraints. The temperature change ΔT and the difference of thermal coefficients $\Delta\alpha$ between the two layers yield $\Delta\varepsilon = \Delta\alpha\Delta T$.

The curvature has been calculated by interpolating a circle on the deformed shape of the upper surface of the cantilever using the Taubin method.[52] The points located along the

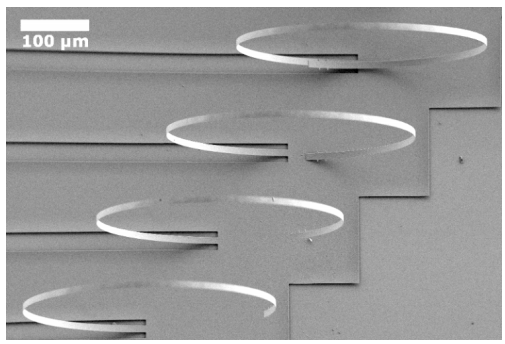

FIG. 2. SEM images of released Si_3N_4/Si bi-layer cantilevers test structures (sample G1).

symmetry axis have been used to quantify the in-length curvature (κ_{axial}). The points located at the half of the cantilever length after reconstruction of the other symmetrical half have been used to quantify the curvature along the width (κ_{transv}). Only the points located at a distance larger than $0.05L$ and $0.1W$ from the edges have been taken into account in order to avoid edge effects. Note that the curvature is indeed constant along the length, but for large values of κ_{transv}, the edge effects affect the entire width of the cantilever. Since the corners have curvatures equal to the one predicted by the small deformation theory, the curvatures presented here are a mean of the local curvature, higher than the curvature at the center, but lower than at the edges.

IV. THEORETICAL BACKGROUND AND DATA REDUCTION SCHEME

A bilayer cantilever of length L and width W is composed of a film of thickness h_f deposited on a supporting material of thickness h_s. It involves an elastic mismatch strain difference $\Delta\varepsilon$ between the film and the supporting layer. After release, the bilayer cantilever bends in order to minimize strain energy and fulfill force and moment equilibrium. The resulting curvature is obviously dependent on $\Delta\varepsilon$, but also on the material stiffness and on the geometry of the cantilever. The assumptions of perfect bonding and of thermal isotropy have been made throughout the work, as well as the linear elastic behavior of the two materials. The main parameters which influence the final curvature of the cantilever are addressed in this section. These results are then used to build the data reduction methodology which has been applied on the experimental measurements for the determination of the elastic modulus and of the internal stress of the layers.

A. Small deformation

The final curvature κ of the bilayer cantilever as a function of $\Delta\varepsilon$ is analytical in the case of equibiaxial conditions, based on forces and momentum equilibrium[8,53,54] or on the minimization of the energy of the system.[2,55] The underlying additional assumptions entering the derivation are small deformation, elastic isotropy, and cantilever geometry where the thickness is much smaller than the width and length. Under these assumptions, the curvatures along the length and along the width are equal and given by

$$\kappa_{axial} = \kappa_{transv} = 6\frac{E_f^* E_s^* \left(h_f + h_s\right)\Delta\varepsilon}{E_f^{*2}h_f^4 + 4E_f^* E_s^* h_f^3 h_s + 6E_f^* E_s^* h_f^2 h_s^2 + 4E_f^* E_s^* h_f h_s^3 + E_s^{*} h_s^4}, \quad (1)$$

where E^* stands for the biaxial modulus ($E^* = E/(1-\nu^2)$ with ν the Poisson ratio and E the Young's modulus), with subscripts f and s referring, respectively, to the film and to the supporting layer. This expression can be written in normalized form as follows:

$$\kappa_{axial} = \kappa_{transv} = \frac{6\Delta\varepsilon\overline{E}\,\overline{h}}{h_s}\frac{\overline{h}+1}{1+\overline{h}\overline{E}\left(4+6\overline{h}+4\overline{h}^2\right)+\overline{h}^4\overline{E}^2}, \quad (2)$$

where $\overline{E} = E_f^*/E_s^*$ is the modulus ratio and $\overline{h} = h_f/h_s$ is the thickness ratio. If it is assumed that $\Delta\varepsilon = \varepsilon_f$ (i.e., $\varepsilon_s = 0$) and converting the latter into the internal stress using $\sigma_f = \varepsilon_f E_f^*$, then the first term becomes simply $6\sigma_f h_f E_s^*/h_s^2$. This expression is known as Stoney's formula,[14,15] which is valid when the stiffness of the substrate is much larger than the stiffness of the film.

B. Large displacements

The promotion of large displacement and significant curvatures is advantageous in order to extend the sensitivity range of the curvature measurement technique and to improve the accuracy, especially in the case of extremely thin layers. But the assumption of small deformation cannot be made and relationship (1) is not valid anymore. Indeed, under large deflections, the curvature does not vary linearly with $\Delta\varepsilon$ anymore.[2,53,55,56] This is shown in Figure 3 which plots the normalized curvature as a function of $\Delta\varepsilon$ for several thickness ratios $\overline{h}$ and for several ratios $W/(h_f + h_s)$. Furthermore, at even larger displacements, the curvature becomes too high to be accommodated equibiaxially when $\Delta\varepsilon$ gets sufficiently large. A bifurcation from spherical to ellipsoidal shape occurs, i.e., axial and transverse curvatures are not equal to one another anymore.[2,8,53,55,57] Contrary to the small deformation case where only $\overline{E}$ and $\overline{h}$ are necessary to predict the evolution of

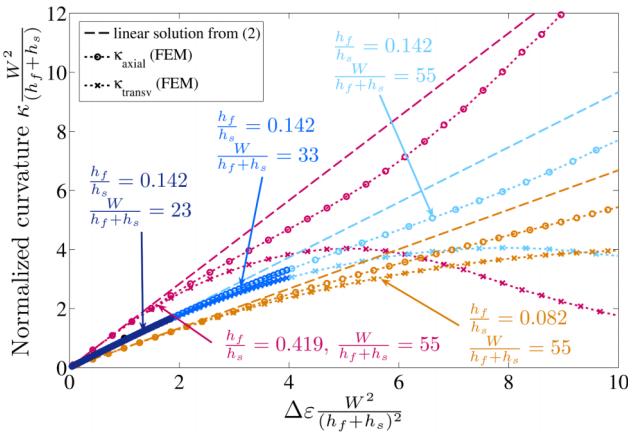

FIG. 3. Effect of the cantilever geometry on the normalized curvature as a function of the normalized mismatch strain difference. The dashed straight lines correspond to the curvature as predicted from Equation (2), the dotted curves with the circles and crosses correspond to, respectively, the axial and the transverse curvature as calculated by FE. The Young's modulus of the film was taken to be 270 GPa.

the curvature with $\Delta\varepsilon$, absolute dimensions and geometry of the cantilever have to be taken into account, too. As shown in Ref. 57, the expression for the critical curvature at bifurcation is of the following form:

$$\kappa_c = \frac{h_f + h_s}{W^2}\overline{\kappa}_c\left(\frac{W}{L}, \overline{h}, \overline{E}\right), \tag{3}$$

where $\overline{\kappa}_c\left(\frac{W}{L}, \overline{h}, \overline{E}\right)$, is a dimensionless function. This expression justifies the choice of the normalization of the curvature that shall be used in the sequel,

$$\overline{\kappa} = \frac{W^2}{h_f + h_s}\kappa, \tag{4}$$

where $\overline{\kappa}$ is the normalized curvature. As shown in Ref. 53, this choice allows the representation of $\overline{\kappa}$ as a function of the normalized strain $W^2/(h_f + h_s)^2\Delta\varepsilon$ independently of a particular choice of the ratio $(h_f + h_s)/W$. This may be appreciated with the data plotted in Figure 3 where three curves associated to the same thickness ratio $\overline{h} = 0.142$, but different in $W/(h_f + h_s)$ ratios (=23, 33, and 55), superimpose.

The bifurcation is sensitive to the in-plane aspect ratio of the cantilever. Bifurcation occurs at larger curvatures as the width/length ratio increases, as shown in Ref. 53. However, as the W/L ratio decreases, this sensitivity decreases. Indeed, taking the expression for $\overline{\kappa}_c$ derived in Ref. 57 from second-order strain approximations, the dependency in W/L vanishes as W/L tends towards 0, i.e., for long narrow cantilevers. All experimentally tested structures had a W/L ratio between 0.005 and 0.1. It has been checked using numerical simulations that if $W/L \leq 0.1$, the dependency on W/L is indeed negligible. Hence, only simulation results with $L = 200$ μm and $W = 10$ μm (i.e., $W/L = 0.05$) have been used for comparison with the experimental results.

To summarize, the normalized curvature of a long narrow bilayer cantilever is uniquely determined by a function of four parameters: the modulus ratio $\overline{E}$, the thickness ratio $\overline{h}$, the width/thickness ratio $W/(h_f + h_s)$, and the difference in elastic mismatch strain $\Delta\varepsilon$. By using a suitable normalization for the curvature and for the strain, it is possible to reduce the number of independent parameters as follows:

$$\kappa_i\frac{W^2}{h_f + h_s} = f_i\left(\Delta\varepsilon\frac{W^2}{(h_f + h_s)^2}, \frac{h_f}{h_s}, \frac{E_f^*}{E_s^*}\right), \tag{5}$$

where the index i refers to either the axial or the transverse direction. When $W^2/(h_f + h_s)^2\Delta\varepsilon$ tends towards zero, the functions f_{transv} and f_{axial} tend to the following expression derived from (2):

$$f_i\left(\Delta\varepsilon\frac{W^2}{(h_f + h_s)^2} \to 0, \frac{h_f}{h_s}, \frac{E_f^*}{E_s^*}\right) = 6\Delta\varepsilon\left(\frac{W}{h_f + h_s}\right)^2\frac{\overline{E}\,\overline{h}\left(\overline{h} + 1\right)^2}{1 + \overline{h}\overline{E}\left(4 + 6\overline{h} + 4\overline{h}^2\right) + \overline{h}^4\overline{E}^2}. \tag{6}$$

C. Data reduction scheme for extracting the Young's modulus and the mismatch strain difference

For a given bilayer with known geometry, the normalized curvature is a function of two non-dimensional parameters: the ratio of moduli $\overline{E} = E_f^*/E_s^*$ and the normalized mismatch strain difference $W^2/(h_f + h_s)^2\Delta\varepsilon$. Performing the FE calculations with several values of the film Young's modulus and with different temperature changes leads to the iso-curvature maps shown in Figure 4. Note that the FE calculations have been performed taking into account the anisotropy of Si and only the modulus of the film has been varied. The modulus has been normalized for the results presented in Figure 4 by using the biaxial modulus of silicon, i.e., $E_s^* = 180$ GPa.[51] For comparison, the iso-curvature lines as predicted by the small deformation theory (relation (6)) are displayed, as well.

The iso-curvature curve corresponding to the experimentally measured curvature is the locus of points $(\Delta\varepsilon,\overline{E})$ which, for this specific cantilever geometry, matches with the measured curvature. In the sequel, we consider only the axial curvature since it is the one which is measured experimentally. The same approach can be followed with the transverse curvature, although the latter is more difficult to measure experimentally, with lower final accuracy in the identified $\Delta\varepsilon$ and $\overline{E}$ values. Measuring another cantilever with either another thickness ratio or another width/thickness ratio (or both) gives another locus of $(\Delta\varepsilon,\overline{E})$ data. Since the film is the same on the two cantilevers, the mismatch strain difference and the modulus ratio are the same. Hence, the intersection of the two loci provides the value of $\Delta\varepsilon$ and $\overline{E}$. The elastic modulus of the film is retrieved if the substrate modulus is known. In the case the bending of the two cantilevers is small enough to respect the conditions of application of the linear theory, the intersection of the loci can be found via the following second degree equation derived from relation (2):

$$\left[\overline{h}_1^4\kappa_1 - \overline{h}_2^4\kappa_2\gamma\right]\overline{E}^2 + \left[\kappa_1\overline{h}_1\left(4 + 6\overline{h}_1 + 4\overline{h}_1^2\right) - \gamma\kappa_2\overline{h}_2\left(4 + 6\overline{h}_2 + 4\overline{h}_2^2\right)\right]\overline{E} + \varphi = 0, \tag{7}$$

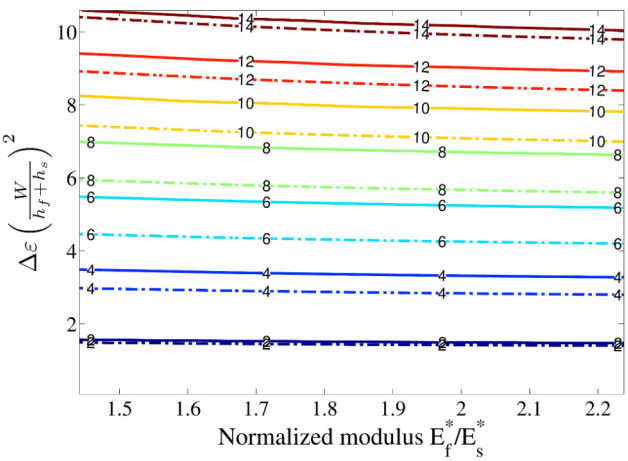

FIG. 4. Axial iso-curvature curves for long cantilevers with $h_f/h_s = 0.419$. The continuous lines represent the normalized curvature as calculated by FE, whereas the dashed lines correspond to the normalized curvature as predicted by analytical expression (6).

where the subscripts 1 and 2 refer to the first and the second cantilevers, $\varphi = \kappa_1 - \gamma\kappa_2$ and $\gamma = \left[\overline{h}_1\left(\overline{h}_1+1\right)h_{s_2}\right] / \left[\overline{h}_2\left(\overline{h}_2+1\right)h_{s_1}\right]$.

V. EXPERIMENTAL VALIDATION

The released freestanding Si monolayer cantilevers did not exhibit any measureable deformation upon release. This indicates the absence of any mismatch strain ε_s in the top Si layer of the SOI wafers. The in-plane displacement of the free LPCVD Si_3N_4 monolayer cantilevers after release involves an average tensile mismatch strain $\varepsilon_f = 0.0032 \pm 0.0001$. Hence, assuming that the Si_3N_4 behaves elastically, the elastic mismatch strain difference between the Si_3N_4 and the Si as extracted from the monolayer cantilevers is given by $\Delta\varepsilon = \varepsilon_f = 0.0032 \pm 0.0001$. No out-of-plane displacement of the free LPCVD Si_3N_4 monolayer cantilevers has been observed, indicating the absence of any strain gradient, as already found in Refs. 13, 18, and 19. Let us mention that the free monolayer cantilevers made of the test material are not essential for applying the present method. Indeed, the production of intact cantilevers of freestanding material can be challenging using solution based etching techniques for thicknesses below 50-100 nm. However, if available, these free monolayer cantilevers made of test material offer a convenient way to check for the presence of a strain gradient inside the film while also offering an independent measurement of the film mismatch strain ε_f.

Table I gives the measured film and substrate thicknesses, as well as the curvature of the bilayer cantilevers in the long direction determined after release. The curvature normalized following expression (4) is also provided. In the sequel, the two series "P" (samples P1, P2, and P3) and "G" (samples G1, G2, G3, and G4) will be treated independently, since the two series "P" and "G" have been produced separately, and might therefore exhibit different properties. All details will be given for the P-series, while only relevant differences will be provided for the G-series.

A. P-series

Figure 5 displays the iso-curvature loci corresponding to the samples of the P-series obtained according to the methodology explained in Section IV C. The intersection points are given in Table II. For comparison, the intersection points obtained if analytical solution (7) is used instead of the FE results are given, as well. The three curves do not intersect at a single point, as it should ideally be the case, but the intersection points form a narrow triangle. The error associated to the curvature measurement indicated in Table I explains a small shift of the iso-curvature lines. The center of gravity of the triangle corresponds to the modulus ratio $E_f^*/E_s^* = 2.06 \pm 0.15$ and to the elastic mismatch strain difference $\Delta\varepsilon = 0.0028 \pm 0.0001$. Figure 6 shows that these values allow the FE results to properly match all the experimental data. The corresponding modulus $E_f = 270 \pm 20$ GPa using $\nu_f = 0.27$ (i.e., a biaxial modulus $E_f^* = 371 \pm 27$ GPa) is in line with the modulus values found in the literature for LPCVD Si_3N_4 (see Table III), although in the upper range. Using the analytical solution instead of the FE results on samples P2 and P3 leads to a modulus ratio and $\Delta\varepsilon$ that are reasonably close to the one found by the FE calculations. But using P1 as one of the two data, combined with the analytical solution, gives results that are totally out of the range. Indeed, as it may be extracted from the data in Figure 3, a deviation of the axial curvature by more than 5% from the analytical solution occurs at a normalized curvature around 1.3-1.5 for the three samples. This is far below the experimentally measured curvature for sample P1, which shows that the analytical solution is absolutely not valid. For sample P3, this limit is much higher than the measured curvature, and therefore the valid use of the analytical solution is granted. Sample P2 has a curvature which is near the value at which the analytical solution is not valid anymore. Using the analytical solution shifts the iso-curvature curve of P2 and causes a slight overestimation of the modulus ratio and an underestimation of $\Delta\varepsilon$ at the intersection point. Hence, using the analytical solution on P2 and P3 induces a limited error and gives already a good estimate of $\overline{E}$ and $\Delta\varepsilon$.

The value for the mismatch strain $\varepsilon_f = \Delta\varepsilon$ agrees with the range of values that have been found using other techniques on similar films. Indeed, the elastic mismatch strain in the film can be converted into an internal stress by $\sigma_f = \varepsilon_f E_f^*$, which gives 1024 ± 30 MPa tensile stress using the measured modulus $E_f^* = 371 \pm 27$ GPa for the biaxial modulus. In Ref. 18, it is reported that tensile stresses for Si_3N_4 deposited exactly in the same conditions are between 795 and 1015 MPa. Moreover, the elastic mismatch strain extracted from free Si_3N_4 cantilevers on the same sample had an average of 0.0032 ± 0.0001 as indicated earlier. Note also that the order of magnitude of $\Delta\varepsilon$ corresponds to the thermally induced strain estimation arising when cooling the sample from the deposition temperature to room temperature, i.e., $(\alpha_{Si} - \alpha_{Si_3N_4})\Delta T \approx 0.0036$, based on $\alpha_{Si} = 7.06\ .010^{-6}\ K^{-1}$ and $\alpha_{Si_3N_4} = 2.3\ .310^{-6}\ K^{-1}$.

TABLE I. Film and substrate thickness, and curvature along the long direction after release of the tested bilayer cantilevers.

	P1	P2	P3	G1	G2	G3	G4
h_f (nm)	54	55	56	46	63	102	133
h_s (nm)	129	388	687	400[a]	400[a]	400[a]	400[a]
h_f/h_s	0.419	0.142	0.082	0.115	0.158	0.255	0.333
$W/(h_f+h_s)$	55	23	13	22	22	20	19
Curvature κ_{axial} (m^{-1})	19 120 ± 450	5744 ± 40	2469 ± 25	5479	6250	7143	7407
Normalized curvature $\overline{\kappa}$	10.4 ± 0.2	1.30 ± 0.1	0.33 ± 0.03	1.23	1.35	1.42	1.39

[a]The values have not been measured and come from the specifications of the SOI wafer.

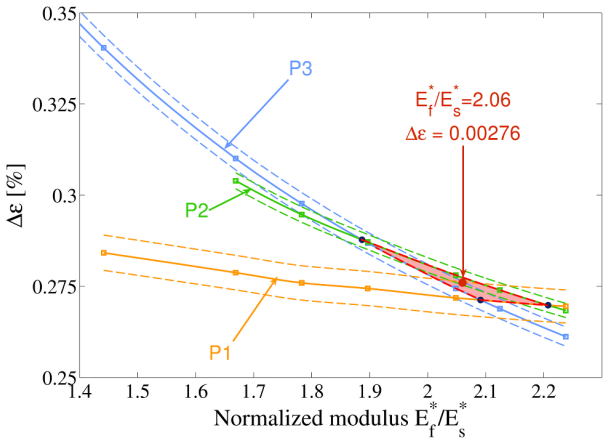

FIG. 5. Iso-curvature curves of the samples of the P-series. The dots correspond to the FE simulations really performed, whereas the lines are spline interpolations as guides for the eye. The dashed lines correspond to the iso-curvature lines taking into account the standard deviation on the curvature.

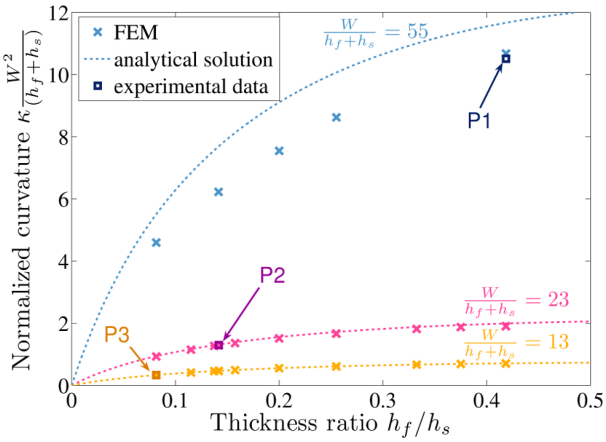

FIG. 6. Normalized curvature as a function of the thickness ratio for $E_f^*/E_s^* = 2.05$ and $\Delta\varepsilon = 0.276\%$.

The width of the beams has not been measured after performing the photolithography and release fabrication steps. It is likely that during the release, the Si_3N_4 and Si layers have been slightly etched also from the side. Moreover, the precision of the photolithography is ±0.5 μm. Since the three samples of the series have been produced in the same run, the error on the width should be the same for all. An error on the width has no consequence on the curvature if the geometry is such that the analytical solution is valid, such as, for instance, for sample P3. But an overestimation of the width when the behavior is not linear anymore (e.g., sample P1) shifts the iso-curvature curve towards the bottom of Figure 5. Redoing the calculation above with $W = 9.5$ μm yields $\Delta\varepsilon = 0.0029 \pm 0.0001$ and $\overline{E} = 1.95 \pm 0.02$, i.e., $E_f = 256 \pm 5$ GPa. An overestimation of the width may partially explain the lower value of $\Delta\varepsilon$ found from the cantilever bending compared with the strain difference extracted from the free monolayer cantilevers.

The Si layer thickness has been measured by ellipsometry. Due to the out-of the-plane bending, the thickness measurements before and after release cannot be made on the released cantilevers themselves. The measurements were performed on zones of the wafer where the Si surface was exposed to the etching solution, hence on zones not covered by the Si_3N_4 film. A difference of 11 nm before and after etching has been measured. Nevertheless, the Si layer in the cantilever is much less exposed to the etching solution than the zones not covered by Si_3N_4. Indeed, the Si will only be etched when the silicon oxide sacrificial layer has been removed. Therefore, the value for h_s that has been used here is most probably a lower bound, and the real value should be nearer to the initial Si layer thickness, i.e., 140, 400, and 700 nm for P1, P2, and P3, respectively. Redoing the calculations using the latter value for h_s leads to $E_f \approx 250$ GPa and $\Delta\varepsilon \approx 0.0029$-$0.0031$. An underestimation of the Si layer thickness may again result in a slightly lower value of $\Delta\varepsilon$ and a slightly higher E_f value in the top of the range found in the literature. Due to the limited access of the etching solution to the Si layer in the cantilevers, the thickness before release is probably a more accurate value for making the calculations. Nevertheless, the two thickness values allow giving lower and upper bounds for E_f and $\Delta\varepsilon$.

TABLE II. Intersection points of the iso-curvature curves of the P-series and G-series.

	Modulus ratio $\overline{E}$		Mismatch strain difference $\Delta\varepsilon$	
	FE	Relation (7)	FE	Relation (7)
P1-P2	2.21	2.88	0.002 70	0.002 41
P1-P3	2.09	2.56	0.002 71	0.002 43
P2-P3	1.89	2.10	0.002 88	0.002 70
Mean	2.06	2.51	0.002 76	0.002 51
Standard deviation	0.13	0.39	0.000 08	0.000 13
G1-G2	2.05	2.13	0.003 00	0.002 89
G1-G3	2.04	2.08	0.003 03	0.002 93
G1-G4	2.00	2.02	0.003 03	0.002 96
G2-G3	2.01	2.04	0.003 01	0.002 94
G2-G4	1.95	1.97	0.003 04	0.002 98
G3-G4	1.89	1.85	0.003 06	0.003 014
Mean	1.99	2.02	0.003 03	0.002 95
Standard deviation	0.06	0.10	0.000 02	0.000 04

The uncertainty on $\Delta\varepsilon$ is less than 4% whereas it is about twice larger for the modulus. This comes from the small slope of the iso-curvature curves, especially for higher h_f/h_s and $W/(h_f + h_s)$ ratios (see Figures 4 and 5). This means that the resulting curvature is much more sensitive to strain variations than to modulus variations for cantilevers with high h_f/h_s and $W/(h_f + h_s)$ ratios. For such structures (like P1), it is possible to estimate $\Delta\varepsilon$ with only one structure, assuming a rough estimate of the modulus.

B. G-series

The same methodology as for the specimens of the P-series has been applied to the samples of the G-series. The intersection points are given in Table II. It yields a Young's modulus $E_f = 261 \pm 8$ GPa and $\Delta\varepsilon = 0.0030 \pm 0.0002$. These values are in excellent agreement with the results determined using the P-series. The analytical solution gives a good estimate of the solution since, as for the specimen P3 previously, the curvature is close to the limit where the actual curvature starts to deviate from the analytical solution. The actual width

TABLE III. A survey of Young's modulus values for LPCVD Si_3N_4 films reported in the literature.

References	Thickness and deposition parameters	Value (GPa)	Measurement method
	100 nm (deposition at 800 °C)	193 ± 20	"Lab-on-chip"
Boé *et al.*[13]	300 nm (deposition at 800 °C)	226 ± 22	"Lab-on-chip"
	500 nm (deposition at 800 °C)	208 ± 18	"Lab-on-chip"
Li and Vlassak[36]	90 nm	224.8 ± 0.8	Nanoindentation
		238.5 ± 1.4	Bulge test
Vlassak and Nix[48]	290 nm (deposition at 785 °C)	222 ± 3	Bulge test
Karimi *et al.*[49]	465 nm	225 ± 10	Bulge test
Madou[58]		270	
Martins *et al.*[59]	104 nm	212 ± 14	Bulge test
Ren and Lam[60]	303–654 nm (deposition at 840 °C and 200 mTorr)	196–309	Cantilever bending
Tabata *et al.*[61]	360 nm	290	Bulge test

W has not been measured on the specimens of the G-series, neither. However, since the behavior is closer to linear, the result is less sensitive to the $W/(h_f + h_s)$ ratio.

For the specimens of the G-series, the substrate thickness after release has not been measured, but has been found in the SOI wafer specifications. Hence, the thickness value is probably slightly overestimated, contrarily to the P-series where it was underestimated.

The proposed approach is valid only under the assumption that the elastic strains are the same in all the specimens. Contrary to the P-series, the film thickness differs between the specimens of the G-series. If there were a strain gradient in the film, then the assumption of the same deposition induced strain in all the specimens would not be valid anymore. Previous measurements showed that there is no evidence of a strain gradient in Si_3N_4 layers.[18] This is also confirmed by the fact that the free monolayer Si_3N_4 cantilevers do not curl. If the strain in the film has another origin than the thermal expansion (e.g., epitaxial growth stress), there might be a strain gradient. Then, the specimens should be designed such that the film on all cantilevers has the same thickness, as in the P-series. Applying the technique to a film with a strain gradient will only lead to a mean strain value.

VI. FINAL DISCUSSION AND CONCLUSION

A new methodology to simultaneously measure the elastic mismatch strain and the Young's modulus of a film deposited on a substrate is proposed, based on cantilever curvature measurements. The objective of this test method is to allow accurate measurements for ultrathin films in the 100 nm thickness range and below. The approach has been applied to 50 to 150 nm thick silicon nitride films, yielding a Young's modulus of 270 ± 20 GPa and a tensile mismatch strain of 0.28 ± 0.01%. This corresponds to an internal stress in the Si_3N_4 film of 1024 ± 30 MPa.

The method relies on the measurement of the curvature of cantilevers with varying thickness ratios h_f/h_s. The intersection of the corresponding iso-curvature curves in the $(E_f^*/E_s^*, \Delta\varepsilon)$ space gives the solution, assuming that the elastic mismatch strain is the same on all the measured cantilevers. From the knowledge of the substrate properties E_s^* and ε_s, it is then possible to retrieve the film properties E_f^* and ε_f. The use of Si as the substrate material is advantageous since its elastic constants are well known and free monolayer cantilevers may be placed on the wafer so as to measure easily ε_s. E_f^* and ε_f are measured simultaneously and the internal stress is obtained directly from $\sigma_f = \varepsilon_f E_f^*$, without the need for an independent modulus measurement.

Theoretically, the "micro-Stoney" method could be applied to any bilayer, without limitation with respect to the support layer and thin specimen material. Beside the accurate knowledge of its elastic constants, the main advantage of using silicon as the substrate is that SOI wafers are commercially available with a variety of thicknesses and of excellent quality. The choice of another substrate material would require the deposition of a sacrificial layer and of the substrate material on a wafer, hence creating more steps, and introducing more experimental uncertainty. The main difficulty concerning the selected materials is not related to the technique itself, but to the fabrication process. Indeed, the release of the bilayers requires chemical etching of the sacrificial layer, here the SiO_2 etched by HF. Selectivity issues of the test and substrate material with respect to the etching solution are an effective limitation with respect to the materials that can potentially be tested, and may require changing the sacrificial layer and the substrate material. Adherence of the test material on the substrate can constitute another limitation. The use of an adherence layer has to be taken into account in the data extraction scheme since the cantilever would become a trilayer and not a bilayer anymore. The stress and the elastic properties of this adherence layer have to be known to adequately retrieve the film properties.

The method can potentially be applied to films as thin as few nanometers, as long as the elastic strain difference between the film and the supporting layer is such that the upper layer is tensile with respect to the supporting layer. Otherwise, the cantilever would bend towards the substrate and would not be allowed to deform properly due to steric hindrance. If the cantilever is long enough and sufficiently bent such that the product of the length by the curvature $L\kappa$ is larger than $\pi/2$, the curvature can be quantified by measuring the loop diameter using SEM. Otherwise, non-contact 3D measurement techniques are needed (e.g., interferometry). In the case of optically transparent films, white light interferometry measurements will cause an overestimation of the radius by an amount equal to the film thickness. However, this error remains small when the films are thin compared to the curvature ratio. In the samples tested here, this

ratio is less than 0.05% and is far below the curvature measurement error.

A better precision in both the Young's modulus value and elastic strain mismatch can be obtained by using cantilevers that give iso-curvature curves with very different slopes. This can be achieved by using cantilevers with very different h_f/h_s ratios. For small normalized curvatures, the curvature is linear with the elastic strain difference and an analytical solution exists, based on the small displacement hypothesis. But for higher curvature values, the analytical solution is not valid anymore and transverse and axial curvatures are no more equal. In this case, FE calculations have to be used to get the iso-curvature curves, and the width/total thickness ratio plays a role in addition to the thickness ratio h_f/h_s. As a consequence, a good precision of the technique requires the knowledge of the film and substrate thickness as well as of the cantilever width after release. Nevertheless, these are ways to decrease the uncertainty but the motivation depends on the accuracy needed with respect to the use that is made of this value in a structural analysis or to compare different deposition conditions, for instance. Theoretically, the technique can work down to a few nanometers film thickness, as recently attempted for graphene in a similar configuration.[62] In this case, it is mainly the accuracy on the thickness that will control the precision of the technique.

ACKNOWLEDGMENTS

The authors acknowledge the financial support of the Walloon Region through the ROMISY and the DINOSAURE projects, the "Communauté Française de Belgique" under the program "Actions de Recherché Concertées" ARC Convention No. 11/16-037, as well as the IAP program of the Belgian State Federal Office for Scientific, Technical, and Cultural Affairs under Contract No. P7/21.The authors are also grateful to Open Engineering and, in particular, to Stéphane Paquay for their help and collaboration.

[1]M. Ohring, *Reliability and Failure of Electronic Materials and Devices* (Academic Press, 1998).
[2]L. B. Freund and S. Suresh, *Thin Film Materials: Stress, Defect Formation and Surface Evolution* (Cambridge University Press, 2003).
[3]M. F. Pantano, H. D. Espinosa, and L. Pagnotta, J. Mech. Sci. Technol. **26**, 545 (2012).
[4]S. Zhang, *Nanostructured Thin Films and Coatings – Mechanical Properties* (CRC Press, 2010).
[5]B. Bushan, *Springer Handbook of Nanotechnology*, 3rd ed. (Springer-Verlag Berlin Heidelberg, 2010).
[6]J. A. Thornton and D. W. Hoffman, J. Vac. Sci. Technol. **14**, 164 (1977).
[7]D. Hoffman and J. A. Thornton, Thin Solid Films **40**, 355 (1977).
[8]T. Clyne and S. Gill, J. Therm. Spray Technol. **5**, 401 (1996).
[9]M. T. Hutchings, *Neutron Diffraction Measurement of Residual Stress Fields: Overview and Points for Discussion* (Kluwer Academic Publishers, 1992).
[10]R. Machunze and G. Janssen, Thin Solid Films **517**, 5888 (2009).
[11]E. Gheeraert, A. Deneuville, A. M. Bonnot, and L. Abello, Diamond Relat. Mater. **1**, 525 (1992).
[12]C. O'Mahony, M. Hill, M. Brunet, R. Duane, and A. Mathewson, Meas. Sci. Technol. **14**, 1807 (2003).
[13]A. Boé, A. Safi, M. Coulombier, T. Pardoen, and J.-P. Raskin, Thin Solid Films **518**, 260 (2009).
[14]G. G. Stoney, Proc. R. Soc. London, Ser. A **82**, 172 (1909).
[15]G. Janssen, M. Abdalla, F. van Keulen, B. Pujada, and B. van Venrooy, Thin Solid Films **517**, 1858 (2009).
[16]Q. Van Overmeere, J.-F. Vanhumbeeck, and J. Proost, Rev. Sci. Instruments **81**, 045106 (2010).
[17]Y. H. Min and Y. K. Kim, J. Micromech. Microeng. **10**, 314 (2000).
[18]J. Laconte, F. Iker, S. Jorez, N. Andre, J. Proost, T. Pardoen, D. Flandre, and J.-P. Raskin, Microelectron. Eng. **76**, 219 (2004).
[19]F. Iker, N. Andre, T. Pardoen, and J.-P. Raskin, J. Microelectromech. Syst. **15**, 1697 (2006).
[20]K. J. Hemker and W. N. Sharpe, Jr., Annu. Rev. Mater. Res. **37**, 93 (2007).
[21]J. Gaspar, M. E. Schmidt, J. Held, and O. Paul, Mater. Res. Soc. Symp. Proc. **1052**, 15 (2008).
[22]T. Tsuchiya, O. Tabata, J. Sakata, and Y. Taga, IEEE. J. Trans. Sens. Micromachines **116**, 441 (1996).
[23]V. Prakash, P. B. Kaul, J. Park, and M. F. P. Bifano, JOM **63**, 49 (2011).
[24]D. Kiener, W. Grosinger, G. Dehm, and R. Pippan, Acta Mater. **56**, 580 (2008).
[25]V. Passi, U. K. Bhaskar, T. Pardoen, U. Sodervall, B. Nilsson, G. Petersson, M. Hagberg, and J.-P. Raskin, Rev. Sci. Instrum. **82**, 116106 (2011).
[26]U. K. Bhaskar, V. Passi, S. Houri, E. Escobedo-Cousin, S. H. Olsen, T. Pardoen, and J.-P. Raskin, J. Mater. Res. **27**, 571 (2012).
[27]M. Coulombier, G. Guisbiers, M.-S. Colla, J.-P. Raskin, and T. Pardoen, Rev. Sci. Instrum. **83**, 105004 (2012).
[28]J. Griffin, F. R. Brotzen, and C. F. Dunn, Thin Solid Films **150**, 237 (1987).
[29]S. Gravier, M. Coulombier, A. Safi, N. Andre, A. Boe, J.-P. Raskin, and T. Pardoen, J. Microelectromech. Syst. **18**, 555 (2009).
[30]M. K. Small, B. J. Daniels, B. M. Clemens, and W. D. Nix, J. Mater. Res. **9**, 25 (1994).
[31]M. Orthner, L. Rieth, and F. Solzbacher, Rev. Sci. Instrum. **81**, 055111 (2010).
[32]H.-J. Kim and Y. G. Kweon, Thin Solid Films **342**, 201 (1999).
[33]W. Oliver and G. Pharr, J. Mater. Res. **19**, 3 (2004).
[34]R. Saha and W. D. Nix, Acta Mater. **50**, 23 (2002).
[35]X. Chen and J. J. Vlassak, J. Mater. Res. **16**, 2974 (2001).
[36]H. Li and J. J. Vlassak, J. Mater. Res. **24**, 1114 (2009).
[37]J. Luo, A. Flewitt, S. Spearing, N. Fleck, and W. Milne, Mater. Lett. **58**, 2306 (2004).
[38]Y. C. Tai and R. S. Muller, *Micro Electro Mechanical Systems, 1990 Proceedings, An Investigation of Micro Structures, Sensors, Actuators, Machines and Robots* (IEEE, 1990), p. 147.
[39]L. Kiesewetter, J.-M. Zhang, D. Houdeau, and A. Steckenborn, Sens. Actuators, A **35**, 153 (1992).
[40]J. S. Burdess, A. J. Harris, D. Wood, R. J. Pitcher, and D. Glennie, J. Microelectromech. Syst. **6**, 322 (1997).
[41]S. Houri, U. Bhaskar, B. Gallacher, L. Francis, T. Pardoen, and J.-P. Raskin, Exp. Mech. **53**, 441 (2003).
[42]M. Alfano and L. Pagnotta, NDT&E Int. **40**, 112 (2007).
[43]J. C. Crowhurst, G. R. Hearne, J. D. Comins, A. G. Every, and P. R. Stoddart, Phys. Rev. B **60**, 990 (1999).
[44]P. A. Mante, J. F. Robillard, and A. Devos, Appl. Phys. Lett. **93**, 071909 (2008).
[45]A. Devos, S. Sadtler, P.-A. Mante, A. Le Louarn, and P. Emery, Appl. Phys. Lett. **105**, 231905 (2014).
[46]P. M. Osterberg and S. D. Senturia, J. Microelectromech. Syst. **6**, 107 (1997).
[47]H. Sadeghian, C. K. Yang, J. F. L. Goosen, E. van der Drift, A. Bossche, P. J. French, and F. van Keulen, Appl. Phys. Lett. **94**, 221903 (2009).
[48]J. J. Vlassak and W. D. Nix, J. Mater. Res. **7**, 3242 (1992).
[49]A. Karimi, O. R. Shojaei, T. Kruml, and J. L. Martin, Thin Solid Films **308-309**, 334 (1997).
[50]K. R. Williams, J. Microelectromech. Syst. **12**, 761 (2003).
[51]M. A. Hopcroft, W. D. Nix, and T. W. Kenny, J. Microelectromech. Syst. **19**, 229 (2010).
[52]G. Taubin, IEEE Trans. Pattern Anal. Mach. Intell. **13**, 1115 (1991).
[53]M. Finot and S. Suresh, J. Mech. Phys. Solids **44**, 683 (1996).
[54]A. Mézin, Surf. Coat. Technol. **200**, 5259 (2006).
[55]L. B. Freund, J. Mech. Phys. Solids **48**, 1159 (2000).
[56]N. J. Salamon and C. B. Masters, Int. J. Eng. Sci. **31**, 915 (1993).
[57]N. J. Salamon and C. B. Masters, Int. J. Solids Struct. **32**, 473 (1995).
[58]M. Madou, *Fundamentals of Microfabrication* (CRC Press, USA, 1997).
[59]P. Martins, C. Malhaire, S. Brida, and D. Barbier, Microsyst. Technol. **15**, 1343 (2009).
[60]Y. Ren and D. C. Lam, Mater. Sci. Eng. A **467**, 93 (2007).
[61]O. Tabata, K. Kawahata, S. Sugiyama, and I. Igarashi, Sens. Actuators **20**, 152 (1989).
[62]H. Conley, N. V. Lavrik, D. Prasai, and K. I. Bolotin, Nano Lett. **11**, 4748 (2011).